Int. J. Electrochem. Sci., 15 **(2020)** 6238 – 6248, doi: 10.20964/2020.07.17

International Journal of
ELECTROCHEMICAL
SCIENCE
www.electrochemsci.org

Low Temperature Electrochemical Synthesis of Nanostructured ZrC Powder in Molten Salt

Hongxia Liu[1,*], *Weihao Song*[1], *Qian Xu*[2,*], *Wen Ma*[1], *Yu Bai*[1]

[1] School of Materials Science and Engineering, Inner Mongolia University of Technology, Inner Mongolia Key Laboratory of Thin Film and Coatings, Hohhot 010051, Inner Mongolia, PR China
[2] State Key Laboratory of Advanced Special Steel, Shanghai University, Shang hai 200072, PR China.
[*]E-mail: pghx@163.com, qianxu@shu.edu.cn

Received: 2 March 2020 / *Accepted:* 14 April 2020 / *Published:* 10 June 2020

ZrC powder was directly electrosynthesized from inexpensive ZrO_2 and carbon black precursors in molten $CaCl_2$-NaCl at 800 °C. Constant voltage electrolysis was applied at 3.1 V between a graphite anode and a cathode composed of a ZrO_2/carbon mixture. The reaction pathway of the solid state reduction was investigated by characterizing the composition and microstructure of partially and fully reduced samples. The spontaneous formation of the intermediate compound $CaZrO_3$ was studied by an immersion experiment and thermodynamic analysis. The results show that the as-synthesized ZrC was composed of spherical particles with an average particle size of roughly 50 nm. The reduction pathway started by converting m-ZrO_2 to $CaZrO_3$, ZrC_xO_{1-x} and t,c-ZrO_2. The phases of t,c-ZrO_2 and $CaZrO_3$ were then reduced to ZrC_xO_{1-x}, which was subsequently reduced to ZrC by the removal of oxygen and in situ carbonization.

Keywords: ZrC; electrochemical; ZrO_2; molten salt

1. INTRODUCTION

Zirconium carbide (ZrC), as a typical member of ultra-high temperature ceramics (UHTCs), possesses many excellent properties such as a high melting point (3540 °C), solid-state phase stability, high hardness, excellent corrosion and wear resistance, good thermal and electrical conductivities, low neutron absorption cross-section and good irradiation resistance. Due to these excellent properties, ZrC is widely used for cutting tools, grinding wheels and abrasives. In addition, it has attracted much attention for potential use in ultra-high temperature applications for hypersonic aerospace flight, atmospheric re-entry vehicles and rocket engines. It is also a promising candidate as an inert matrix material and refractory fuel coating material in the nuclear industry[1-5]. Furthermore, the mechanical properties of the metallic matrix can be markedly improved by adding nanosized ZrC particles[6-8].

Several methods have been developed to synthesize ZrC powder including carbothermal reduction of zirconium dioxide[9,10], self-propagating high-temperature synthesis (SHS)[1], preceramic polymer method[11], mechanical alloying[12] and mechanochemical synthesis[13]. Among them, the primary preparation route is carbothermal reduction due to inexpensive raw materials, simple process and low investment. However, this process requires high temperature (above 1400 ℃) and long reaction durations, which leads to relatively large particle sizes (e.g. micrometer scale) and poor sinterability of the final product[2,11]. Shape and size of the product limit its wide applications. The sinterability and mechanical properties of the product could be markedly improved by reducing the ZrC particle size down to the nanoscale[3,4]. The other aforementioned methods have made efforts to reduce the size of ZrC. However, high cost precursors, hazardous substances, expensive active metals, impurity of the products, or complicated processes are typically involved in most cases. A simple, cost-effective, non-toxic and relatively low temperature technique is desired to synthesize ZrC nanoparticles. In recent years, the electro-deoxidation process, as a novel and effective method, has been used to synthesize refractory metals, semi-metals or alloys from solid metal oxides[14-17]. This method has obvious advantages such as requiring inexpensive precursors, a simple route and a relatively low reaction temperature. Recently, the preparation of nanosized powders of refractory metal carbides (e.g., NbC, TiC and HfC) has been attempted from metal oxides/carbon precursors[18-20]. However, there are only few studies on the electrochemical synthesis of nanosized zirconium carbide.

In this study, nanosized zirconium carbide was synthesized by an electro-deoxidation process in molten chlorides using the cheapest zirconium-bearing precursor, zirconium dioxide, in the presence of nano carbon black at 800 ℃. The detailed electrochemical pathway from the sintered ZrO_2/C precursor to ZrC was also investigated. The goal of the present work was to obtain uniformly dispersed nanosized ZrC powder using a simpler approach from low cost and environment-friendly precursors at relatively low temperature.

2. EXPERIMENTAL

A mixture of commercial ZrO_2 (AR, China National Pharmaceutical Group Co., Ltd) and nano carbon black with a molar ratio of 1:1 was ball milled in anhydrous alcohol for 4 h. The powder mixture was then pressed into a cylindrical pellet (Ø15×1 mm) under 8 MPa of pressure. The pellet was sintered at 900 °C for 4 h under a continuous flow of argon gas and then connected to a stainless steel wire to assemble the cathode. A high-density graphite rod (Ø10×60 mm) served as the anode. A $CaCl_2$-NaCl eutectic mixture (AR, Tianjin Kemiou Chemical Reagent Co., Ltd.) was used as the electrolyte. It was packed in an alumina crucible and dehydrated at 300 °C for 24 h.

The alumina crucible filled with the mixed salt was introduced into the stainless steel reaction vessel. Then, the vessel was sealed and filled with argon gas. The reactor was heated to the target temperature of 800 ℃ with argon gas circulation. The salt was subjected to pre-electrolysis at 2.5 V for 2 h to remove any electrochemically active impurities. The electrolysis experiments were conducted at 3.1 V between the anode and the cathode. After electrolysis, the

samples were carefully rinsed with distilled water several times to remove the salt, and subsequently dried at 80 ℃ before characterization.

Identification of the phase composition of the sample was carried out by X-ray diffraction (XRD, Rigaku D/Max-2500PC). The morphology and chemical composition of the sample were determined using a field-emission scanning electron microscope (FESEM, CarlZeiss-EVO18) coupled with energy-dispersive X-ray spectroscopy (EDX).

3. RESULTS AND DISCUSSION

Carbon black and graphite are two kinds of abundantly available carbon sources. As shown in Fig. 1a and b, the carbonization reaction by amorphous carbon has a more negative value of ΔG^{θ} compared to graphite between 500 to 1500 ℃. Hence, carbon black, a kind of amorphous carbon, is more active towards carbonization of zirconium than graphite according to the thermodynamic analysis. Since carbon atoms are obviously smaller than Zr atoms, the diffusion that occurs during the carbonization process can be mainly attributed to the migration of carbon atoms[21]. Theoretically, smaller size of carbon particles is beneficial for the diffusion during carbonization due to the larger contact area and the shorter diffusion distance. Therefore, nano carbon black was selected as the carbon source in this study.

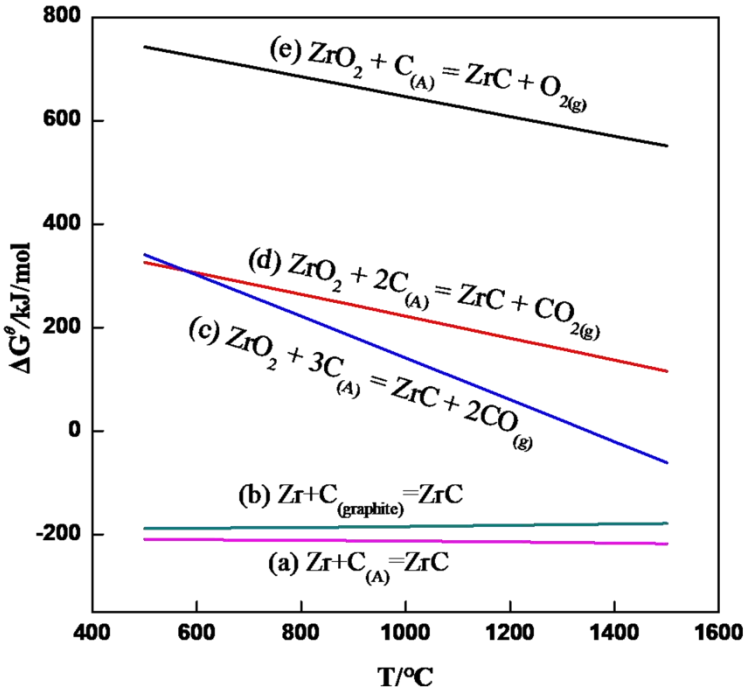

Figure 1. Standard Gibbs energy for different reactions as a function of temperature

ZrO_2 and carbon black powders were mixed in a 1:1 molar ratio, then compacted and sintered in an Ar atmosphere at 900 ℃ for 4 h. The XRD pattern of the sintered pellet is shown in Fig. 2 a. A

single-phase of m-ZrO_2 is observed, and the diffraction peaks of carbon are not be detected, which may be due to the amorphous structure of the carbon additive used in this study. The obtained results indicate that no chemical reaction occurs between ZrO_2 and carbon during sintering. In theory, the carbothermal reactions (CTR) of ZrO_2 can take place via reactions (1)-(3). The standard Gibbs free energy of the reactions is shown in Fig. 1 c-e, which reveals that the testing temperature (900 °C) is too low for the CTR reactions to occur. Therefore, the carbon black powder likely serves as a carbon source for generating carbides instead of a reducing agent during the electro-reduction process at 800℃. Fig. 2b displays the morphology of the ZrO_2/C sintered pellet. It is clearly seen that the micron sized ZrO_2 particles are surrounded by nano carbon particles, and the two kinds of particles are evenly mixed together. In addition, the pellet is porous, which is beneficial for the liquid phase mass transfer.

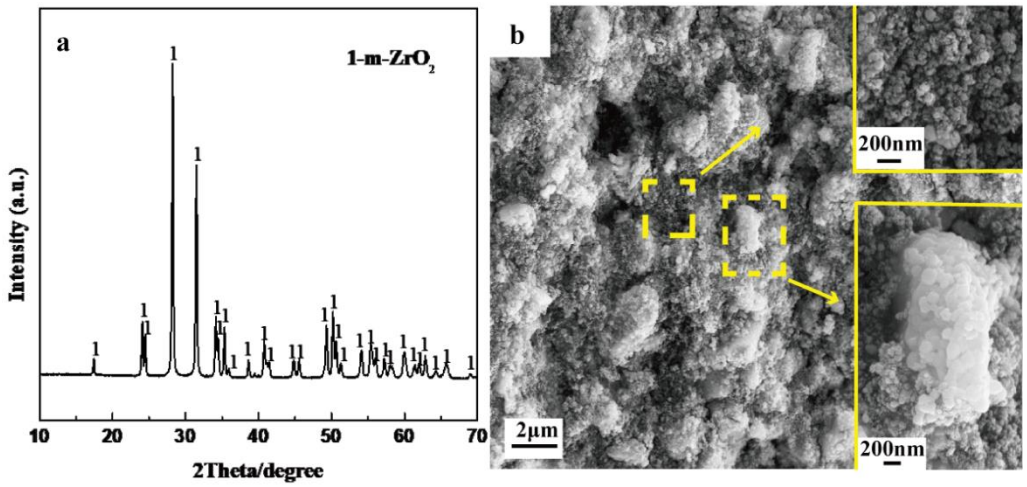

Figure 2. (a) XRD pattern; (b) SEM image of ZrO_2/C mixed pellets sintered at 900 °C for 4 h

$$ZrO_2 + C_{(Amorphous)} = ZrC + O_{2(g)} \quad (1)$$

$$ZrO_2 + 2C_{(Amorphous)} = ZrC + CO_{2(g)} \quad (2)$$

$$ZrO_2 + 3C_{(Amorphous)} = ZrC + 2CO_{(g)} \quad (3)$$

A preliminary investigation was conducted to evaluate the effect of submerging the ZrO_2/C sintered pellets in molten salt. As shown in Fig. 3a, the sample after immersion in molten $CaCl_2$-NaCl for 30 h is composed of $CaZrO_3$, which results from the reaction between ZrO_2 and CaO, as given by Eq. (4). Some CaO was inevitably formed due to the hydrolysis of Ca^{2+} when calcium chloride was thermally dried[22,23], and readily dissolved in molten $CaCl_2$-NaCl[24].

$$ZrO_2 + (CaO)_{CaCl_2} = CaZrO_3 \qquad \Delta G^{\theta}_{T=800℃} = -34.95 \ \ kJ{\cdot}mol^{-1} \quad (4)$$

The Gibbs free energy change (ΔG) for reaction (4) can be expressed as:

$$\Delta G = \Delta G^{\theta} + RT\ln\frac{a_{CaZrO_3}}{a_{ZrO_2}\cdot a_{CaO}} \quad (5)$$

where a_{CaZrO_3}, a_{ZrO_2} and a_{CaO} are the activities of $CaZrO_3$, ZrO_2 and CaO, respectively, and T and R are the temperature (K) and the ideal gas constant, respectively. The term ΔG^{θ} is the standard

Gibbs free energy of reaction (4) and is equal to -34.95 kJ·mol^{-1} at 800 °C[25]. The two solid compounds of ZrO_2 and $CaZrO_3$ can be assumed to have unit activities, because they are almost insoluble in the melt. Therefore, $a_{CaZrO_3} = a_{ZrO_2} = 1$. If the activity coefficient (γ_{CaO}) and the mole fraction (x_{CaO}) of dissolved CaO are substituted into Eq. (5), it can be re-written as Eq. (6):

$$\Delta G = \Delta G^{\theta} + RT\ln\frac{1}{\gamma_{CaO}\cdot x_{CaO}} \qquad (6)$$

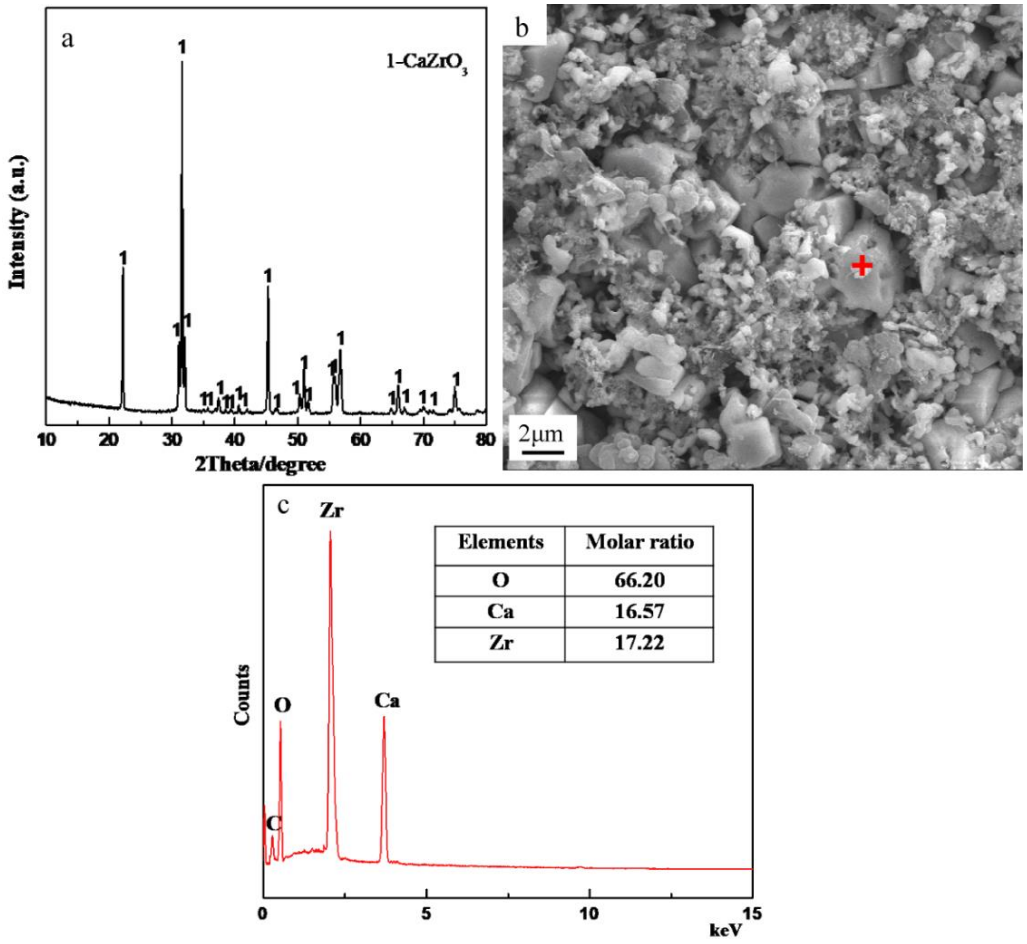

Figure 3. (a) XRD pattern; (b) SEM image of ZrO_2/C sintered pellets immersed in molten $CaCl_2$-NaCl at 800 °C for 30 h; as well as (c) EDS spectrum obtained from the marked point in (b)

Here, γ_{CaO} in molten $CaCl_2$-NaCl is approximately equal to 13.07 at 800°C, and the air dried $CaCl_2$ contains 0.4-0.79 mol% CaO according to the literatures[19,26]. The activity of CaO in the CaCl-NaCl melt is estimated to be 0.05-0.10. Therefore, the calculated ΔG for reaction (4) is less than zero, indicating that $CaZrO_3$ is formed spontaneously once the ZrO_2/C sintered pellet is immersed into molten $CaCl_2$-NaCl at 800 °C. Besides, the ionized O^{2-} can be released from the ZrO_2/C cathode by the electro-deoxidation process and dissolves into the $CaCl_2$-based melt. Consequently, there is local enrichment of CaO or (O^{2-} and Ca^{2+}) within or near the porous cathode, thereby facilitating the formation of $CaZrO_3$. Hence, it can be predicted that $CaZrO_3$ is inevitably formed during the electro-

deoxidation process. Based on the SEM micrograph and EDS analysis (Fig. 3b and c), it is clearly seen that the formed $CaZrO_3$ particles are block-shaped with an approximate size of 2 μm.

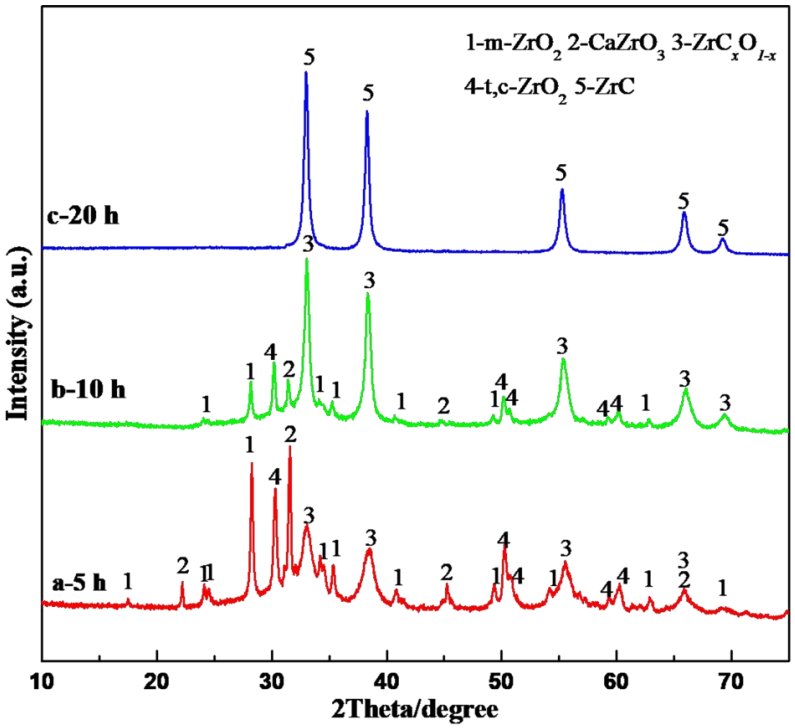

Figure 4. XRD patterns of samples electrolyzed under 3.1 V at 800 °C in molten $CaCl_2$-NaCl for (a) 5 h; (b) 10 h; (c) 20 h

The cathodes of ZrO_2/C sintered pellets were electrolyzed under 3.1 V at 800 °C for different times. Various phases of the cathode products after electrolysis were identified by XRD, as shown in Fig. 4. After the first 5 h of reduction, the sample is primarily composed of $CaZrO_3$, m-ZrO_2 and t,c-ZrO_2, and the remaining XRD peaks are ascribed to ZrC. However, the diffraction peaks indexed to ZrC are shifted to higher angles. The lattice parameter of the carbide phase is 0.4686 nm, which is markedly smaller than that of stoichiometric ZrC (0.47 nm), as shown in Fig. 5. This is generally considered to be characteristic of the presence of oxygen in the carbide lattice, forming a cubic oxycarbide phase of ZrC_xO_{1-x}. It is widely accepted that monoclinic form of ZrO_2 (m-ZrO_2), tetragonal form (t-ZrO_2) and cubic form (c-ZrO_2) are stable below 1170, 1170-2370 and above 2370 ℃, respectively[27,28]. The appearance of the t, c-ZrO_2 phase indicates that the transition from m-ZrO_2 to t, c-ZrO_2 occurs at 800 ℃ in molten salt. This result can be explained as follows: (1) the local temperature around the cathode rises due to the exothermic carbonization reaction, which leads to crystal transformation; (2) carbon in the cathode can help stabilize c-ZrO_2 at lower temperatures[27]. The c-ZrO_2 phase has higher ionic conductivity, which is beneficial to the transfer of O^{2-} generated by electro-deoxidation. The following reactions (7)-(11), in addition to reaction (4), are proposed to occur at the cathode. The theoretical potentials for these possible reactions were calculated from thermodynamic data[25], as shown in Table 1. To simplify the calculation, the stoichiometric ZrC was

chosen to replace all the oxycarbide phases. According to thermodynamic analysis, it can be deduced that the cathodic reactions (10) and (11) with the lowest cathodic potentials are the preferred electrochemical reactions at the molten salt/cathode interface, followed by the dissolution of ionized O^{2-} into the melt.

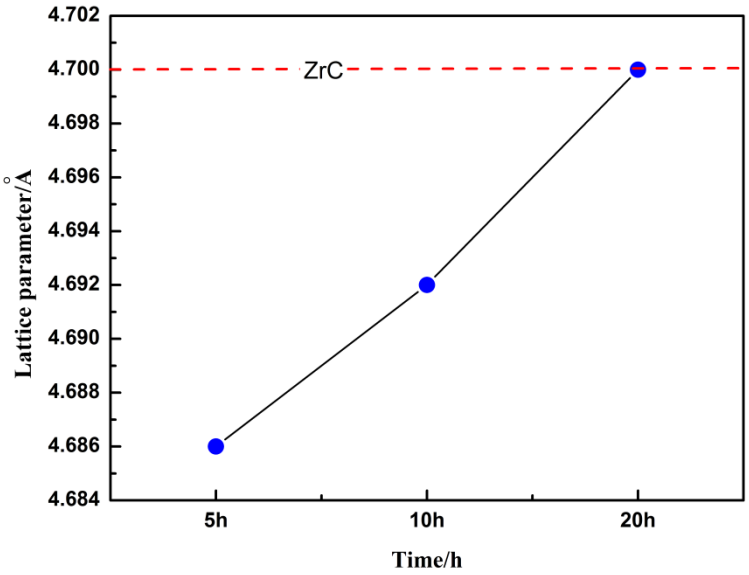

Figure 5. Changes in lattice parameters of the ZrC_xO_{1-x} phase under varying electrochemical reduction durations

$$ZrO_2 + 4e = Zr + 2O^{2-} \quad (7)$$

$$CaZrO_3 + 4e = Zr + CaO + 2O^{2-} \quad (8)$$

$$Zr + C = ZrC \quad (9)$$

$$ZrO_2 + 2(1+x)e + xC = ZrC_xO_{1-x} + (1+x)O^{2-} \quad (10)$$

$$CaZrO_3 + 2(1+x)e + xC = ZrC_xO_{1-x} + Ca^{2+} + (2+x)O^{2-} \quad (11)$$

After 10 h of reduction, the XRD spectrum shows a decrease in peaks indexed to ZrO_2 and $CaZrO_3$ and an increase in peaks ascribed to ZrC_xO_{1-x}, whose position gradually shifts to lower angles with time. This result suggests that ZrC_xO_{1-x} is formed at the expense of ZrO_2 and $CaZrO_3$. The value of the cell parameter of ZrC_xO_{1-x} increases slightly, as shown in Fig. 5, indicating that the content of oxygen in the ZrC_xO_{1-x} phase decreases. As the electrolysis time increases to 20 h, the peaks of ZrO_2 and $CaZrO_3$ diminish and the product is composed of a single-phase ZrC, indicating that all the tetravalent zirconium compounds are reduced to the ZrC phase. This stage is typically characterized by the reduction of ZrC_xO_{1-x} to ZrC, as shown in Eq. (12). Additionally, it has been reported that ZrC powder was synthesized at 1527 °C and 1300°C, respectively, by modified carbothermal reaction method [29] and polymerized complex route [30]. Therefore, the synthesis temperature of ZrC powder in this work is much lower than that by carbothermal reaction and polymerized complex methods.

$$ZrC_xO_{1-x} + 2(1-x)e + (1-x)C = ZrC + (1-x)O^{2-} \quad (12)$$

Table 1. Theoretical decomposition voltage of possible reactions at 800 ℃

Reactions	Theoretical decomposition voltage (E_r,V)
$ZrO_2=Zr+O_{2(g)}$	2.3
$CaZrO_3=Zr+ O_{2(g)}+CaO$	2.4
$ZrO_2+C=ZrC+O_{2(g)}$	1.8
$CaZrO_3+C=ZrC+ O_{2(g)}+CaO$	1.9

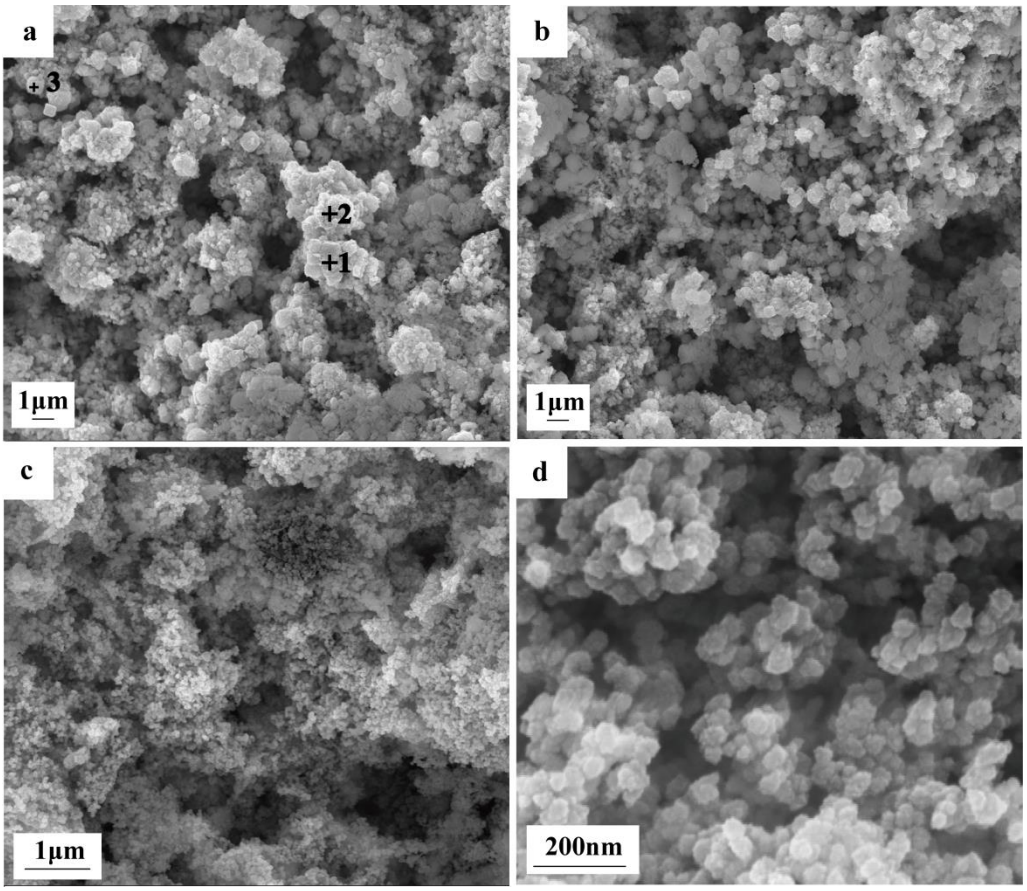

Figure 6. SEM images of samples electrolyzed at 800 °C in $CaCl_2$-NaCl melt for (a) 5 h; (b)10 h; (c) and (d) 20 h

Fig. 6 shows the SEM images for samples after different electro-deoxidation durations. Several types of particles are observed in the sample after 5 h reduction, as shown in Fig. 6a. A few cube-like particles and nodular particles newly emerge, compared to the sample before electrolysis (Fig. 2b and 3b). According to the XRD (Fig. 4a) and EDS (Fig. 7) analyses, the large irregular particles about 2 μm in size are m-ZrO_2 or $CaZrO_3$, whereas the cube-like particles with an average size of less than 1 μm are t,c-ZrO_2. The relatively fine nodular particles should be composed of carbide phases. The particle sizes of the intermediate phases are smaller than or equal to that of the initial m-ZrO_2. Fig. 6b shows the SEM image of the sample after 10 h reduction. It can be seen that the larger particles are converted into smaller ones, and more fine nodular particles are observed. This result indicates that

more carbide phases are produced at the cathode due to the gradual electro-deoxidation and the subsequent carbiding. Fig. 6c-d shows that the obtained ZrC is composed of homogeneous spherical grains with a size of about 50 nm. The particle size of ZrC powder obtained in this work is smaller than that of ZrC grains synthesized by modified carbothermal reaction method (170 nm) [29] and polymerized complex method (50-150 nm) [30].

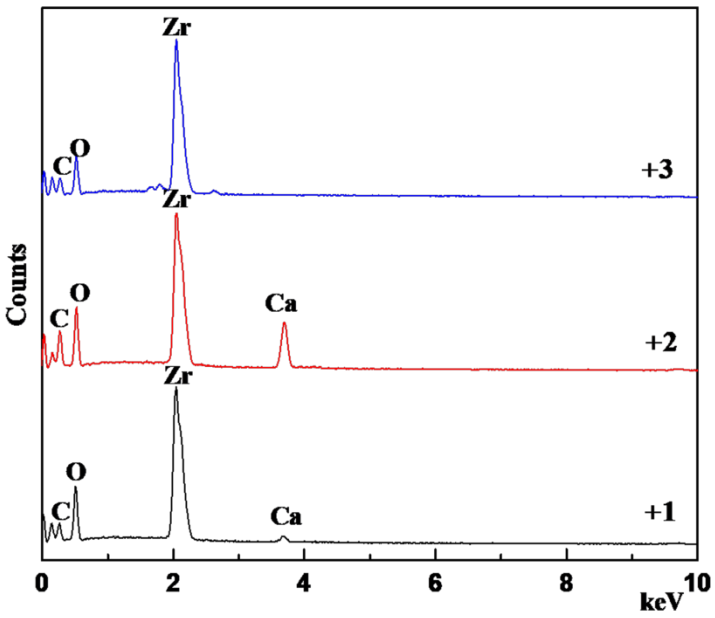

Figure 7. EDX spectra obtained from analysis of points 1, 2 and 3 labeled in Figure 6a

According to the above results, the electrochemical reduction of the ZrO_2/C mixture generates nanosized ZrC powder in molten $CaCl_2$-NaCl. A schematic illustration of the reaction pathway is shown in Fig. 8. The formation of ZrC involves several intermediate steps. After the ZrO_2/C pellet is immersed into the melt and the cathodic overpotential is applied, m-ZrO_2 is converted into the intermediate phases of $CaZrO_3$ and t,c-ZrO_2. Meanwhile, the tetravalent zirconium compounds are reduced to the oxycarbide phase ZrC_xO_{1-x} by the synergetic reactions of oxygen removal and carbonization. With the further formation and successive reduction of intermediate phases, the pellet is reduced to ZrC_xO_{1-x}. Finally, the content of oxygen in the ZrC_xO_{1-x} phase gradually decreases until stoichiometric ZrC is formed.

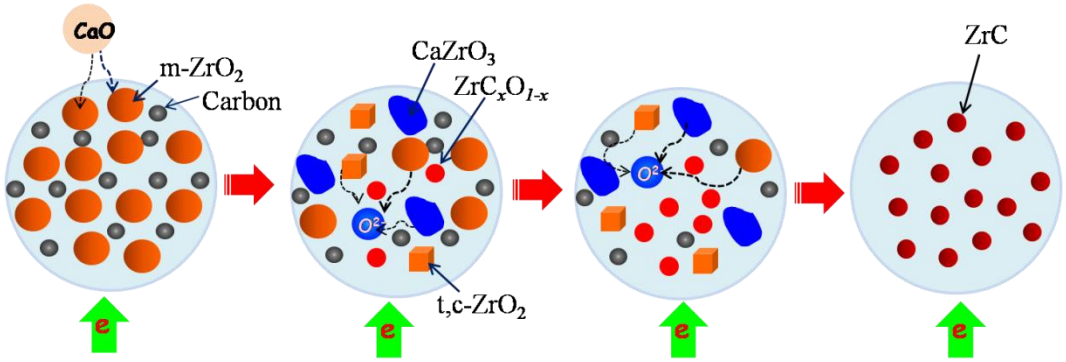

Figure 8. Schematic illustration of the electrolytic synthesis of nanosized zirconium carbide in molten salt.

4. CONCLUSIONS

In this work, zirconium carbide powder with particle size of approximately 50 nm was synthesized by the electrochemical reduction process from low cost ZrO_2/carbon black precursors in molten $CaCl_2$-NaCl under 3.1 V at 800 °C. It was found that a perovskite phase of $CaZrO_3$ was spontaneously formed due to the chemical reaction between ZrO_2 and CaO once the ZrO_2/C pellet was immersed into $CaCl_2$-based molten salt. A series of interrupted electrolytic experiments in combination with thermodynamic calculations were conducted to investigate the mechanism of the electrolysis process. The results indicated that the electro-reduction pathway consisted of the following three steps: (1) electrochemical reduction of m-ZrO_2 in the presence of carbon to form ZrC_xO_{1-x}, accompanied by the formation of intermediate phases such as $CaZrO_3$ and t,c-ZrO_2; (2) reduction of the tetravalent zirconium intermediate compounds together with synergetic carbonization to form ZrC_xO_{1-x}; and (3) removal of oxygen from ZrC_xO_{1-x} to form ZrC.

ACKNOWLEDGEMENTS
This work was funded by the Higher Educational Scientific Research Projects of Inner Mongolia Autonomous Region (Grant No.NJZZ19066), Natural Science Foundation of Inner Mongolia Autonomous Region(Grant No.2019MS05066), and Science and Technology Major Project of Inner Mongolia Autonomous Region (Grant No.2018-810).

References

1. M. X. Zhang, Q. D. Hu, B. Huang and J. G. Li, *Alloys Compd*., 509 (2011) 8120.
2. Danial Davoodia, S. A. Hassanzadeh-Tabrizia, Amir Hossein Emami and Saman Salahshour, *Ceram. Int*., 41 (2015) 8397.
3. Y.J. Yan, Z.R. Huang, X.J. Liu and D.L. Jiang, J. Sol-Gel Sci. Technol., 2007, 44(1), 81-85.
4. J. X. Wang, D. W. Ni, S. M. Dong, G. Yang, Y. F. Gao, Y. M. Kan, X. W. Chen, Y. P. Cao and X. Y. Zhang, *RSC Adv.*, 7 (2017), 22722.
5. K. Li, X. Zhou, Z. Zhao, C. Chen, C. Wang, B. Ren and L. Zhang, *J. Solid State Chem.*, 258 (2018) 383.
6. W. S. Tian, D. S. Zhou, F. Qiu, Q. C. Jiang, *Mater. Sci. Eng*. A, 658 (2016) 409.

7. J. B. Ferguson, F. Sheykh-Jaberi, C. S. Kim, P. K. Rohatgi and K. Cho, *Mater. Sci. Eng*. A, 558 (2012) 193.
8. K. B. Nie, X. J. Wang, X. S. Hu, L. Xu, K. Wu and M. Y. Zheng, *Mater. Sci. Eng*. A, 528 (2011) 5278.
9. A. Maitre and P. Lefort, *Solid State Ionics*, 104 (1997) 109.
10. M. D. Sacks, C. A. Wang, Z. Yang and A. Jain, *J. Mater. Sci*., 39 (2004) 6057.
11. X. Y. Tao, W. F. Qiu, H. Li and T. Zhao, *Polym. Adv. Technol.*, 21 (2010) 300.
12. J. Y. Xiang, S. C. Liu, W. T. Hua, Y. Zhang, C. K. Chen, P. Wang, J. L. He, D. L. Yu, B. Xu, Y. F. Lu, Y. J. Tian and Z. Y. Liu, *J. Eur. Ceram. Soc.*, 31 (2011) 1491.
13. D. Davoodi, S. A. Hassanzadeh-Tabrizi, A. H. Emami and S. Salahshour, *Ceram.Int.*, 41 (2015) 8397.
14. J. Peng, H. Chen, X. Jin, T. Wang, D. Wang and G. Z. Chen, *Chem. Mater*., 21 (2009) 5187.
15. R. Bhagat, M. Jackson, D. Inman and R. Dashwood, *J. Electrochem. Soc.,* 155 (2008) E63.
16. W. Xiao, J. Zhou, L. Yu, D. Wang, and X. W. Lou, *Angew. Chem. Int. Ed.*, 55 (2016) 1.
17. G. H. Qiu, D. H. Wang, M. Ma, X. B. Jin and G. Z. Chen, *J. Electroanal. Chem*., 589 (2006) 139.
18. A. M. Abdelkader and D. J. Fray, *J. Eur. Ceram. Soc*., 32 (2012) 4481.
19. X. Y. Yan, M. I. Pownceby, M. A. Cooksey and M. R. Lanyon, *Trans. Inst. Min Metall*. C, 118 (2009) 23.
20. Q. S. Song, Q. Xu, J. C. Meng, T. P. Lou, Z. Q. Ning, Y. Qi and K. Yu, *Alloys Compd*., 647 (2015) 245.
21. I. DahanU, U. Admon, N. Frage, J. Sariel and M. P. Dariel, *Thin Solid Films*, 377 (2000) 687.
22. G. Z. Chen and D. J. Fray, *J. Electrochem. Soc*., 149 (2002) E455.
23. C. Schwandt and D. J. Fray, *Electrochim. Acta*, 51 (2005) 66.
24. R. O. Suzuki, M. Aizawa and K. Ono, *J. Alloys Compd.,* 288 (1999) 173.
25. A. Roine, HSC Chemistry, version 6.0, Outokumpu Research Oy, Pori, Finland, 2006.
26. S. Wang, F. Zhang, X. Liu and L. Zhang, *Thermochim. Acta*, 470 (2008) 105.
27. T. Y. Luo, T. X. Liang and C. S. Li, *Mater. Sci. Eng*., A, 366 (2004) 206.
28. Lj. Kljajevic, B. Matovic, A. Radosavljevic-Mihajlovic, M. Rosic, S. Boskovic and A. Devecerski, *Alloys Compd*., 509 (2011) 2203.
29. E. Cetinkaya, *J. Am. Ceram. Soc.*, 100 (2017) 5444.
30. R. Liu, C. Yan, C. Zhang, Y. Cao and X. Long, *Adv Appl Ceram*, 115(1) (2016) 6.